mathematics

MDPI

Article

Computational Insights into the Unstable Fixed Point of the Fractional Difference Logistic Map

Ernestas Uzdila, Inga Telksniene, Tadas Telksnys and Minvydas Ragulskis *

Department of Mathematical Modelling, Kaunas University of Technology, Studentu 50-147, LT-51368 Kaunas, Lithuania; ernestas.uzdila@ktu.edu (E.U.); inga.telksniene@ktu.lt (I.T.); tadas.telksnys@ktu.lt (T.T.)
* Correspondence: minvydas.ragulskis@ktu.lt

Abstract: Thedivergence from the unstable fixed point of the fractional difference logistic map is investigated in this paper. In contrary to the classical logistic map, the memory horizon of the fractional difference logistic map reaches the initial condition. And though higher order orbits do not exist in the fractional difference logistic map, a trajectory started at the unstable fixed point may continuously remain at the fixed point as the number of iterations tends to infinity. Such an effect is well known for the classical logistic map, but less so in the fractional difference logistic map. It appears that this effect depends on the accuracy of the floating point arithmetic. It is demonstrated that the divergence from the unstable fixed point of the fractional difference logistic map is a completely computational artifact. Using double precision, approximately 32% values of a from the interval $2.7 < a \leq 3.7$ diverge from the unstable fixed point.

Keywords: periodic orbit; stability; fractional derivative; logistic map

MSC: 37C25; 37E05; 39B12; 26A33

Citation: Uzdila, E.; Telksniene, I.; Telksnys, T.; Ragulskis, M. Computational Insights into the Unstable Fixed Point of the Fractional Difference Logistic Map. *Mathematics* **2024**, *12*, 3635. https://doi.org/10.3390/math12233635

Academic Editor: Nicolae Herisanu

Received: 10 October 2024
Revised: 14 November 2024
Accepted: 19 November 2024
Published: 21 November 2024

1. Introduction

Computer simulations of complex nonlinear systems often raise questions about the origin of the observed numerical effects. Are those effects the artifacts of the simulation algorithms, or do they reflect the inherent physical properties of the modeled systems?

Chaotic dynamics is indeed an integral feature of many nonlinear systems. However, numerical precision and rounding errors may affect the outcomes of simulations of chaotic systems [1–5]. In particular, numerical methods used for the simulation of fractional systems must account for the non-local nature of fractional derivatives, which may significantly increase the computational complexity [6–8].

One of the paradigmatic mathematical models capable of exhibiting complex chaotic dynamics is the classical logistic map [9]. It is used in a myriad of applications, ranging from computer science (encryption, random number generation) [10,11], physics (chaos theory, phase transitions) [12,13], biology (population dynamics, epidemiology) [14,15], to medicine (cardiac dynamics and neuroscience) [16,17].

The fractional difference logistic map utilizes Caputo differences rather than classical differences [18–20]:

$$x_{n+1} = x_0 + \sum_{j=1}^{n+1} G_{j-1}^{\mu} \left(a x_{n-j+1} \left(1 - x_{n-j+1} \right) - x_{n-j+1} \right), j = 0, 1, \ldots, \tag{1}$$

where $G_0^{\mu} = 1, G_j^{\mu} = \left(1 - \frac{1-\mu}{j}\right) G_{j-1}^{\mu}, j = 1, 2, \ldots$. The parameter $\mu \in (0, 1]$ describes the fractionality of (1), and setting $\mu = 1$ results in the classical logistic map.

The key feature of the fractional maps lies in their ability to represent the memory effects [21,22]. In fact, the memory horizon of the fractional difference logistic map (1)

extends all the way back to the initial condition, making it well-suited for applications where the system's historical evolution significantly influences its future dynamics [23,24].

The fractional difference logistic map possesses a number of important features. For example, it is shown that the iterations necessary to avoid transients must be in the order of thousands and not hundreds [23]. While this is not unique to fractional maps (see [2,25]), this is nonetheless essential to acknowledge when considering such systems. Moreover, it has been shown in [26] that the convergence times to an unstable fixed point prior to bifurcations may exponentially depend on initial conditions.

Peculiarities of the chaotic behavior of the fractional difference logistic map are investigated in [27–29]. The cascade of bifurcations in the fractional difference logistic map, including the analysis of parameter values at which period-doubling bifurcations occur, has been investigated in [30]. Trajectories in which a cascade of bifurcations occurs—not as a result of a change in a system's parameter, but on a single attracting trajectory during its time evolution—are noted and explored in fractional maps in [30]. Chaos control of the fractional difference logistic map is discussed in [31,32].

It is entirely natural that all reported numerical simulations of the fractional difference logistic map are conducted using floating-point arithmetic. This raises the question: do the numerical algorithms used for identifying specific trajectories and the stabilization of the fractional map accurately reflect the dynamics of the system or are the observed features of the fractional difference logistic map just numerical artifacts? For example, will setting the initial condition to the unstable fixed point of the fractional difference logistic map always yield a fixed trajectory during its time evolution? Some of these questions may seem elementary; however, further investigation reveals that the apparent simplicity of the problem is misleading.

The study of the influence of computational errors on nonlinear dynamical systems is a classical topic, with the most common problem being determining how integration (iteration) steps interact with system parameters. However, in this paper, a completely different problem is considered: rather than studying the influence of computational errors on the iterations of the map, we analyze the effect that standard floating-point computation systems (such as a finite number of significant digits) on the behavior of the unstable fixed point, which can only be represented in finite precision due to floating-point limitations. Addressing these questions is the primary objective of this paper.

The paper is structured as follows. Section 2.1 investigates the unstable equilibria of the classical logistic map. Section 2.2 clarifies the classification of the values of the parameter a . Sections 2.3–2.5 discuss the brute force and Monte Carlo methods for classifying unstable period-1 and period-2 orbits. Section 3 examines the unstable fixed point of the fractional difference logistic map. Finally, concluding remarks are provided in the last section.

This structure is tightly related to the methodology applied in this study: firstly, the Types of different a values with respect to the divergence/convergence properties of the fixed point are defined for a given floating-point precision. Next, and algorithm to evaluate the type of any a value is developed and then simplified to a single step. Subsequently, it is proven that this algorithm is also applicable to the fractional difference logistic map and the Monte-Carlo method is used to evaluate proportions of a value Types for high floating-point precision.

2. Unstable Equilibria of the Classical Logistic Map

2.1. Preliminaries and the Motivation of This Study

Consider the classical logistic map [9]:

$$x_{n+1} = ax_n(1 - x_n), \quad n = 0, 1, \ldots, \tag{2}$$

where the parameter of the logistic map $a \in [0, 4]$, and the initial condition $x_0 \in [0, 1]$.

For $1 < a \leq 3$, the map has a single stable equilibrium point representing a period-1 orbit. Thus, representing the value of a inaccurately does not significantly impact the evolution of the map, since all initials converge towards the same period-1 fixed point.

Suppose that $a > 3$ in (2). Then, the equilibrium,

$$x_* = 1 - \frac{1}{a}, \tag{3}$$

representing the period-1 orbit, is unstable. However, x_* remains the equilibrium. Therefore, from the analytical point of view, the initial condition $x_0 = 1 - \frac{1}{a}$ should lead to a period-1 orbit $x_0 = x_1 = x_2 = \cdots = x_*$.

However, in floating-point arithmetic this is not always the case. The representation of x_* is not always completely accurate in floating-point arithmetic. As a result, the initial condition $x_0 = x_*$ does not always lead to a period-1 orbit and diverges from the fixed point x_* (at $a > 3$).

The main objective of this section is to explore when the initial conditions set to the equilibrium points of the unstable orbits does (or does not) yield those unstable orbits when the computations are performed in floating-point arithmetic.

2.2. The Classification of the Values of the Parameter a

Consider a floating-point system that can represent numbers with exactly N significant digits. Throughout the remainder of the text, numbers denoted with a tilde such as $\widetilde{x}_1$ will indicate a value computed using the floating-point arithmetic with N significant digits. Without loss of generality, all further analytical and numerical derivations are performed in decimal numeral system, and standard rounding rules are applied.

Since it is well-known that the results may depend on the rounding mode [33] and order of operations [34], a particular order of operations has been used throughout all numerical experiments. All variables are saved using the `double` variable type; the numbers are rounded to N significant digits after each arithmetic operation, while the order of computational steps follows general mathematical rules.

It appears that the numerical values of the parameter of the logistic map a can be classified into three different Types.

Type-1: The analytical value of x_*, corresponding to the chosen value of the parameter a, is accurately represented in floating-point arithmetic.
Example 1. Let $N = 5$ and $a = \texttt{0.32000} \times \texttt{10}^1$. The analytical value of x_* is 0.6875 according to (3). This value of x_* is accurately represented by $\widetilde{x}_* = \texttt{0.68750} \times \texttt{10}^0$ in floating-point arithmetic at $N = 5$.
The initial condition $x_0 = \widetilde{x}_*$ and the parameter value a yield $x_1 = 0.6875$ according to (2). The computation of x_1 yields the same value $\widetilde{x}_1 = \texttt{0.68750} \times \texttt{10}^0$ in the floating-point arithmetic at $N = 5$. Further iterations can be repeated indefinitely and the trajectory of the logistic map remains fixed at $\widetilde{x}_*$.
Such values of a are denoted as Type-1 values of the parameter a.

Type-2: The analytical value of x_*, corresponding to the chosen value of the parameter a, cannot be accurately represented in floating-point arithmetic at the provided N value, but the trajectory of the logistic map remains fixed at $\widetilde{x}_*$.
Example 2. Let $N = 5$ and $a = \texttt{0.30846} \times \texttt{10}^1$. The analytical value of x_* according to (3) is $x_* = \frac{10423}{15423} = 0.675808856\ldots$. The computation of x_* in the floating-point arithmetic yields $\widetilde{x}_* = \texttt{0.67581} \times \texttt{10}^0$ at $N = 5$.
The initial condition $x_0 = \widetilde{x}_*$ and the parameter value a yield $x_1 = 0.675807617\ldots \neq \widetilde{x}_*$ according to (2). However, the computation of x_1 in the floating-point arithmetic at $N = 5$ yields $\widetilde{x}_1 = \texttt{0.67581} \times \texttt{10}^0 = \widetilde{x}_*$. Further iterations can be repeated indefinitely, with the trajectory of the logistic map remaining fixed at $\widetilde{x}_*$. The trajectory remains fixed at $\widetilde{x}_*$ even though the values $\widetilde{x}_* = \texttt{0.67581} \times \texttt{10}^0$ and $a = 3.0846$ do not formally satisfy (3). This is an effect induced by the finite representation of floating-point numbers. Such values of a are denoted as Type-2 values of the parameter a.

Type-3: The analytical value of x_*, corresponding to the chosen value of the parameter a, cannot be accurately represented in floating-point arithmetic at given N, and the trajectory of the logistic map diverges away from x_*.
Example 3. Let $N = 5$ and $a = \texttt{0.34567} \times \texttt{10}^1$. The analytical value of x_* according to (3) is $x_* = \frac{24567}{34567} = 0.710706743\ldots$, while the computation of x_* in the floating-point arithmetic at $N = 5$ yields $\widetilde{x}_* = \texttt{0.71071} \times \texttt{10}^0$.
Note that the Type-4 value of the parameter a (x_* is accurately represented in floating-point arithmetic and the trajectory diverges from x_*) does not exist. The existence of a Type-4 value of the parameter a would contradict the definition of the fixed point.
The initial condition $x_0 = \widetilde{x}_*$ and the parameter value a yield $x_1 = 0.710701999\ldots \neq \widetilde{x}_*$ according to (2). Moreover, the computation of x_1 in the floating-point arithmetic at $N = 5$ yields $\widetilde{x}_1 = \texttt{0.71070} \times \texttt{10}^0 \neq \widetilde{x}_*$. The following iterations produce a sequence diverging from $\widetilde{x}_*$. Such values of a are denoted as Type-3 values of the parameter a.

The definitions and derivations presented above are illustrated in Table 1.

Table 1. The computational illustration of the three different types of the parameter a (at $N = 5$). The three values of a have been selected arbitrarily to represent each different Type of point. The Type-1 value of a yields the values of x_*, $\widetilde{x}_*$, x_1, and $\widetilde{x}_1$ represented exactly in the floating point arithmetic. The values of x_* and x_1 cannot be exactly represented in the floating point arithmetic for the Type-2 value of a. However, the floating-point arithmetic (at $N = 5$) yields $x_* = \widetilde{x}_1 = \widetilde{x}_2 = \ldots$. The Type-3 value of a yields a diverging trajectory from $\widetilde{x}_1$.

Type	a	x_*	$\widetilde{x}_*$	x_1	$\widetilde{x}_1$
Type-1	$\texttt{0.32000} \times \texttt{10}^1$	0.6875	$\texttt{0.68750} \times \texttt{10}^0$	0.6875	$\texttt{0.68750} \times \texttt{10}^0$
Type-2	$\texttt{0.30846} \times \texttt{10}^1$	0.675808856...	$\texttt{0.67581} \times \texttt{10}^0$	0.675807617...	$\texttt{0.67581} \times \texttt{10}^0$
Type-3	$\texttt{0.34567} \times \texttt{10}^1$	0.710706743...	$\texttt{0.71071} \times \texttt{10}^0$	0.710701999	$\texttt{0.71070} \times \texttt{10}^0$

2.3. Type-1 Values of a for the Unstable Period-1 Orbit

Note that for $3 < a \leq 4$, the initial condition is bounded in $\frac{2}{3} \leq x_* < \frac{3}{4}$. Therefore, the leading digit before the decimal point for x_* is always 0. The value of a in the decimal system can be expressed analytically as:

$$a = \frac{A}{10^N} = \frac{\alpha}{\beta}, \quad \gcd(\alpha, \beta) = 1, \tag{4}$$

where A is an integer from the interval $\left(3 \cdot 10^N, 4 \cdot 10^N\right]$; $\alpha, \beta \in \mathbb{N}$ represent the numerator and the denominator of the fraction $\frac{A}{10^N}$. Now,

$$x_* = 1 - \frac{1}{a} = \frac{B}{10^N} = \frac{\alpha - \beta}{\alpha}, \quad B \in \left[2.5 \cdot 10^{N-1}, \mathrm{round}(3.\overline{3} \cdot 10^{N-1})\right). \tag{5}$$

Note that it is required that $\beta = 2^{l_1}5^{l_2}$; $l_1, l_2 \in \mathbb{N}$ for (4) to hold true. If A and 10^N do not share common factors, $\beta = 2^N5^N$. If A and 10^N do share common factors, then the powers of 2 and 5 in the integer factorization of β are reduced.

Following the same reasoning, the numerator of a must be $\alpha = 2^{k_1}5^{k_2}$ (the same number is the denominator of x_*). Also, the number must be fully represented with $N + 1$ significant digits.

Thus, for $x_0 = x_*$ to result in a trajectory that remains at this point as $n \to +\infty$, the value of a must be expressed in the following form:

$$a = \frac{2^{k_1}5^{k_2}}{2^{l_1}5^{l_2}}, \tag{6}$$

$k_1, k_2 \in \mathbb{N}$. Now let us consider four cases:

Case 1: Let $k_1 < l_1$ and $k_2 < l_2$. Then $a = \dfrac{1}{2^{l_1-k_1}5^{l_2-k_2}} < 3$, which is out of bounds, since $a \in (3, 4]$.

Case 2: Let $k_1 > l_1$ and $k_2 > l_2$. Then $a = 2^{k_1-l_1}5^{k_2-l_2} > 4$, which is out of bounds, since $a \in (3, 4]$.

Case 3: Let $k_1 \leq l_1$ and $k_2 \geq l_2$. Then $a = \dfrac{5^{k_2-l_2}}{2^{l_1-k_1}}$.

Case 4: Let $k_1 \geq l_1$ and $k_2 \leq l_2$. Then $a = \dfrac{2^{k_1-l_1}}{5^{l_2-k_2}}$.

The above cases show that there are only 4 possible values of a which are Type-1 values of a. These values, along with respective x_* and their decimal representations are given in Table 2.

Table 2. Type-1 values of a and the corresponding values of the unstable fixed points x_* in analytic and decimal representations.

Value of a	$\frac{25}{8}$	$\frac{16}{5}$	$\frac{125}{32}$	4
Decimal form of a	$3.125\overline{0}$	$3.2\overline{0}$	$3.90625\overline{0}$	$4.\overline{0}$
Fixed point x_*	$\frac{17}{25}$	$\frac{11}{16}$	$\frac{93}{125}$	$\frac{3}{4}$
Decimal form of x_*	$0.68\overline{0}$	$0.6875\overline{0}$	$0.744\overline{0}$	$0.75\overline{0}$

The above points are the only Type-1 values of a that exist only for a sufficiently high value of N. For $N \geq 6$, all four Type-1 values of a do exist because the longest decimal representation of a or x_* uses at most 6 significant digits.

2.4. Unstable Period-1 Orbit; $3 < a \leq 4$

2.4.1. The Brute Force Approach

In this and all subsequent sections, floating-point computations are performed using exactly N significant digits for each arithmetical operation.

The brute force approach is based on the computational classification of all possible values of $3 < a \leq 4$ at given $N \geq 2$. Firstly, all possible floating-point representations of $3 < a \leq 4$ are generated at a given value of N. The set of these floating-point values of a is denoted as $S_a(N)$. Next, for each value $a \in S_a(N)$, the corresponding value of $\widetilde{x}_*$ is computed. Subsequently, an initial condition of $x_0 = \widetilde{x}_*$ is set and one iteration $\widetilde{x}_1$ of the logistic map is calculated. If $\widetilde{x}_1 \neq x_0$, then the respective value of a is considered a Type-3 value; otherwise, if a is not one of the Type-1 values listed in Table 2, then it is considered a Type-2 value.

The values of a, $\widetilde{x}_*$ and $\widetilde{x}_1$ for the case of $N = 2$ are given in the Table 3 as an example of the computations outlined above. Table 3, though simple, is not elementary. For example, it appears that the number of red rows in Table 3 is much larger than the number of green rows. Furthermore, red rows do not form a compact set.

It is interesting to observe what the ratio between green rows and red rows is in Table 3 at different values of N. Let us denote this ratio as:

$$\rho(N) = \frac{|S_a^{(1,2)}(N)|}{|S_a(N)|} \cdot 100\% \tag{7}$$

where $S_a^{(1,2)}(N)$ is the set of all values of the parameter a that are either Type-1 or Type-2 at a given N, and the standard modulus sign denotes the cardinality of the set.

Table 3. The classification of the parameter values of a at $N = 2$. Red rows denote diverging trajectories (Type-3 values of a). Green rows denote trajectories remaining at the unstable period-1 orbit (Type-1 and Type-2 values of a). Note that one time-forward iteration is sufficient to determine the type of a.

a	$\widetilde{x}_*$	$\widetilde{x}_1$	Type
3.1	0.68	0.67	Type-3
3.2	0.69	0.68	Type-3
3.3	0.70	0.69	Type-3
3.4	0.71	0.70	Type-3
3.5	0.71	0.73	Type-3
3.6	0.72	0.73	Type-3
3.7	0.73	0.73	Type-2
3.8	0.74	0.73	Type-3
3.9	0.74	0.75	Type-3
4.0	0.75	0.75	Type-1

Table 4 depicts the relation between N and $\rho(N)$. It can be observed that $\rho(9)$ approaches 28.77%. Note that the brute force approach at larger values of N becomes infeasible due to the vastness of $|S_a(N)|$.

Table 4. The relationship between N and $\rho(N)$.

N	1	2	3	4	5	6	7	8	9
$\rho(N)$	0	20	27	29.30	28.47	28.66	28.69	28.75	28.77

2.4.2. The Monte-Carlo Approach

Without loss of generality, let us fix $N = 15$. A Monte-Carlo method is used to evaluate the proportion of Type-2 values of parameter a. This classical technique is based on random uniform sampling of parameter a values and checking their type. This allows the drawing of conclusions based on the smaller sample rather than all a values, which would be unfeasible to check by brute force [35].

A random number generator is used to uniformly sample the values of a from the interval $(3, 4]$. Let us fix the number of trials to 10^7 ($|S_a(15)| = 10^7$). All further computations are based on the computations explained in the preceding section. It appears that $\rho(15) = 28.77\%$ (Figure 1). In other words, every fourth randomly chosen value of a (in $(3, 4]$) yields a trajectory which remains at the unstable period-1 orbit.

It is interesting to observe how ρ changes at different sub-intervals of $(3, 4]$ (at fixed $N = 15$). The interval $(3, 4]$ is divided into 100 equal sub-intervals. Let $S_{a_k}(15)$ denote all values of a belonging to the k-th sub-interval of $(3, 4]$. Then:

$$S_a(15) = \bigcup_{k=1}^{100} S_{a_k}(15). \tag{8}$$

Now, the ratio of Type-1 and Type-2 values of a in the k-th sub-interval is denoted as $\rho_k(15)$. The distribution of $\rho_k(15)$ in $(3, 4]$ is shown in the form of 100 black horizontal lines in Figure 1. It is interesting to note that the values of $\rho_k(15)$ are larger at the left-hand side, and smaller at the right-hand side of the interval $(3, 4]$ (Figure 1). This effect could be explained by the fact that the period-1 orbit (i.e., the fixed point x_*) is stable for $a < 3$.

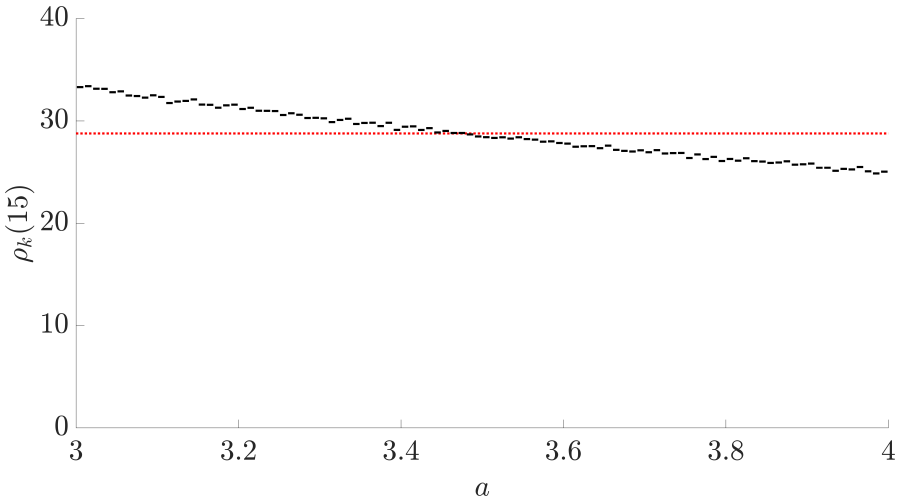

Figure 1. Black dashes depict $\rho_k(15)$, $k = 1, \ldots, 100$. The red horizontal line represents $\rho(15) \approx 28.77\%$. All computations are performed at $N = 15$.

2.5. Unstable Period-2 Orbit; $1 + \sqrt{6} < a \leq 4$

A similar classification can be organised for the unstable period-2 orbit of the classical logistic map. Note that the period-2 orbit $\{x_{*U}; x_{*L}\}$ becomes unstable following the second period-doubling bifurcation at $a = 1 + \sqrt{6}$ (Figure 2), as shown in [36]:

$$x_{*U} = \frac{a + 1 + \sqrt{a^2 - 2a - 3}}{2a}; x_{*L} = \frac{a + 1 - \sqrt{a^2 - 2a - 3}}{2a}. \tag{9}$$

Note that Type-1 values of a do not exist for the unstable period-2 orbit. The classification is now only performed between Type-2 and Type-3 values of a.

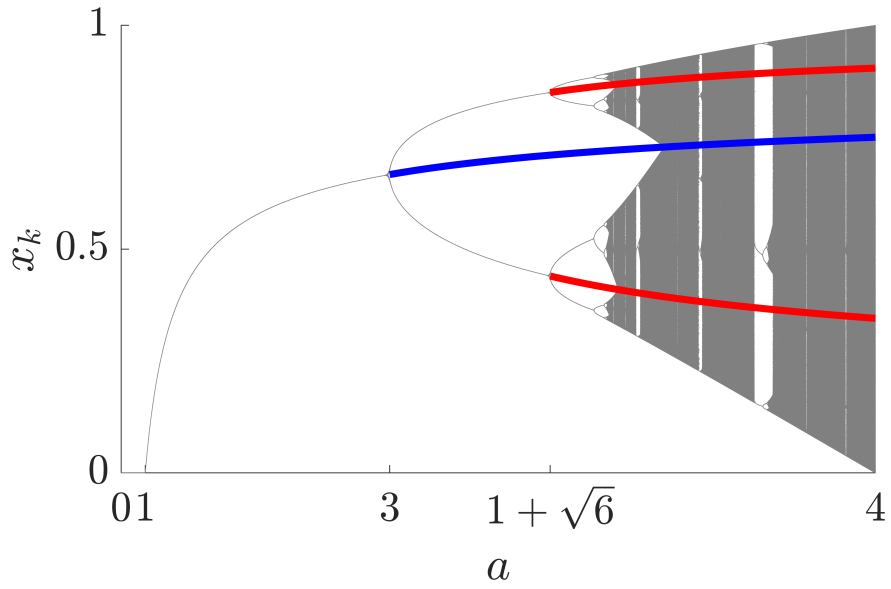

Figure 2. The bifurcation diagram of the classical logistic map. The blue line denotes the unstable period-1 orbit ($3 < a \leq 4$). The red lines denote the unstable period-2 orbit ($1 + \sqrt{6} < a \leq 4$). Note that the a-axis is shown in the logarithmic scale.

2.5.1. The Brute Force Approach

All possible floating-point representations for $1 + \sqrt{6} < a \leq 4$ are generated at a given value of N. The set of these floating-point values of a is denoted by $S_a(N)$. Next, for each value $a \in S_a(N)$, the corresponding values of $\widetilde{x}_{*U}, \widetilde{x}_{*L}$ are computed. Subsequently, the initial conditions of $x_{0U} = \widetilde{x}_{*U}$ and $x_{0L} = \widetilde{x}_{*L}$ are set, and two iterations of the logistic map

are performed for each of the initial conditions, resulting in $\widetilde{x}_{2U}, \widetilde{x}_{2L}$. If these values do not correspond to their respective initial conditions, then they are considered Type-3 values, otherwise they are considered Type-2 values.

Let $S^{(2)}_{aU}(N)$ and $S^{(2)}_{aL}(N)$ denote the sets of all Type-2 values of the parameter a for the upper and lower branches of the period-2 orbit, respectively. Then, the ratios of Type-2 values of the parameter a for the upper and lower branches of the period-2 orbit at given N are denoted as:

$$\rho_U(N) = \frac{|S^{(2)}_{aU}(N)|}{|S_a(N)|} \cdot 100\%; \quad \rho_L(N) = \frac{|S^{(2)}_{aU}(N)|}{|S_a(N)|} \cdot 100\%. \tag{10}$$

Table 5 depicts the relationship between $\rho_U(N)$, $\rho_L(N)$, and N. It can be observed that $\rho_U(9)$ approaches 11.00%, while $\rho_L(9)$ approaches 4.89%. Note that the brute force approach at larger values of N becomes unfeasible due to the vastness of $|S_a(N)|$.

Table 5. The relationship between $\rho_U(N)$, $\rho_L(N)$, and N.

N	**1**	**2**	**3**	**4**	**5**	**6**	**7**	**8**	**9**
$\rho_U(N)$	0	14.29	10.71	10.33	9.99	11.15	10.97	11.00	11.00
$\rho_L(N)$	0	0	1.79	5.43	4.49	5.04	4.93	4.93	4.89

2.5.2. The Monte-Carlo Approach

Without loss of generality, let us fix $N = 15$. A random number generator is used to uniformly sample the values of a from the interval $[1 + \sqrt{6}, 4]$. Let us fix the number of trials to 10^7 ($|S_a(15)| = 10^7$). Note that all values of a are represented by $N = 15$ significant digits. While it is possible to repeatedly sample the same values, the likelihood of this is negligible. All further computations are based on the approach presented in the previous section. It appears that $\rho_U(15) = 8.95\%$ and $\rho_L(15) = 5.07\%$ (Figure 3).

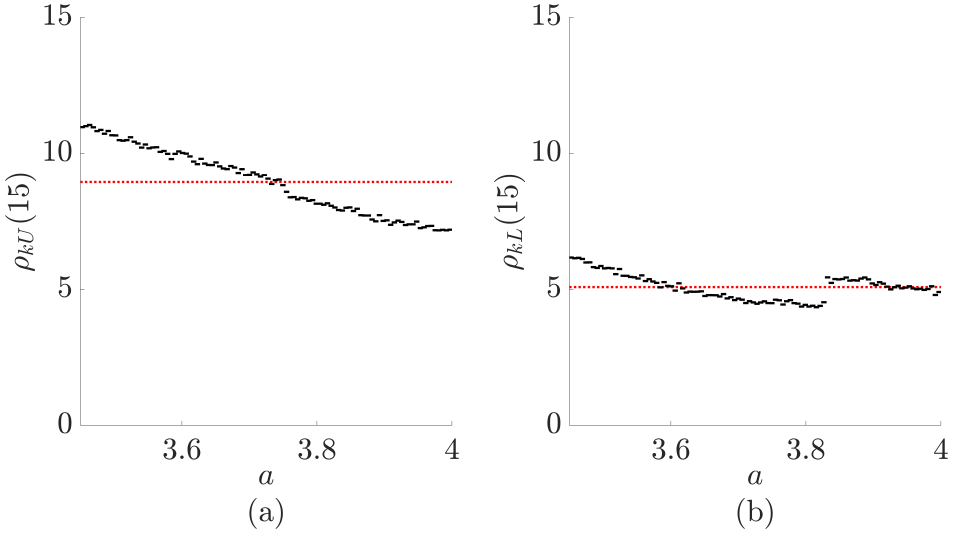

Figure 3. Black dashes depict $\rho_{kU}(15)$ (part (**a**)) and $\rho_{kL}(15)$ (part (**b**)), $k = 1, \ldots, 100$. The red horizontal lines represents $\rho_U(15) \approx 8.95\%$ (part (**a**)) and $\rho_L(15) \approx 5.07\%$ (part (**b**)). All computations are performed at $N = 15$.

It is interesting to observe how ρ changes at different sub-intervals of $[1 + \sqrt{6}, 4]$ (at fixed $N = 15$). The interval $[1 + \sqrt{6}, 4]$ is divided into 100 equal sub-intervals. Let $S_{a_k}(15)$ denote all values of a belonging to the k-th sub-interval of $[1 + \sqrt{6}, 4]$.

Now, the ratios of Type-2 values of a in the k-th sub-interval are denoted as $\rho_{kU}(15)$ and $\rho_{kL}(15)$. The distributions of $\rho_{kU}(15)$ and $\rho_{kL}(15)$ in $[1 + \sqrt{6}, 4]$ are shown in the form

of 100 black horizontal lines in Figure 3. It can be observed that $\rho_{kU}(15)$ has a general decreasing trend as a increases, while $\rho_{kL}(15)$ does not match this exactly: at around $a = 3.82$ it appears to jump up and then continue to decrease. Such effects can be attributed to regularity windows around otherwise chaotic regimes.

3. The Fractional Difference Logistic Map

It is well known that the fractional difference logistic map does not have periodic orbits, except for fixed points [37]. However, this fact does not rule out the existence of a fixed point (the period-1 orbit).

Let us consider the fixed point of the classical logistic map: $x_* = 1 - \frac{1}{a}$ (3). Then, setting $x_0 = x_*$ yields (according to (1)):

$$\begin{aligned} x_1 &= x_* + G_0^\mu(x_* - x_*) = x_*; \\ x_2 &= x_* + G_0^\mu(x_* - x_*) + G_1^\mu(x_* - x_*) = x_*; \\ &\ldots \end{aligned} \tag{11}$$

Therefore, the classification of the parameter a values for the unstable period-1 orbit of the fractional difference logistic map is identical to the classical logistic map, except for the fact that the fixed point x_* becomes unstable already at a = $2^\mu + 1$, as shown in Equation (46) of [38] which, in this case, corresponds to approximately $a \approx 2.7$.

The red dots in Figure 4 indicate such values of a (in the interval $2.7 < a \leq 3.7$) where the trajectory remains at the fixed point (Type-2 values of a) at $N = 15$ and $\mu = 0.8$. The computationally reconstructed value of $\rho(15)$ is 32%. In other words, almost every third randomly chosen value of a from the interval $2.7 < a \leq 3.7$ yields a trajectory which always remains at the fixed point $\widetilde{x}_*$. The other two thirds of values of a yield trajectories diverging from $\widetilde{x}_*$ (Figure 5).

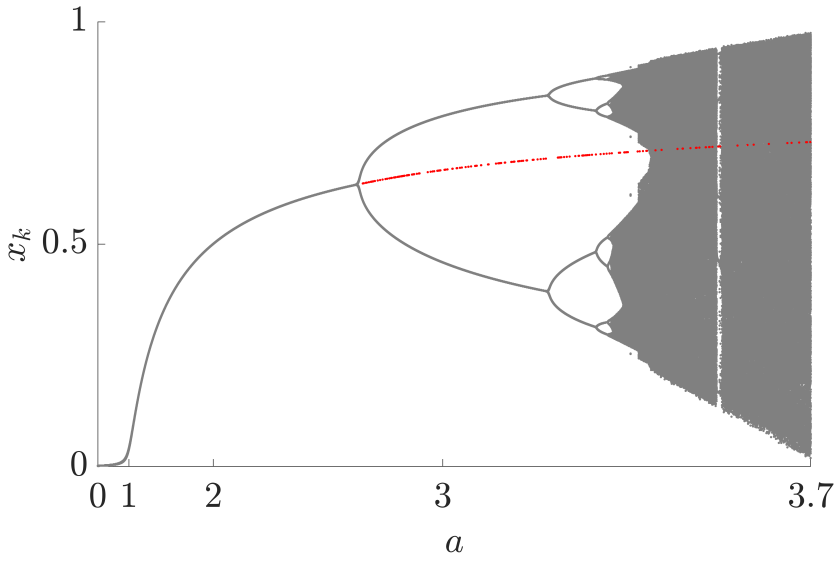

Figure 4. The bifurcation diagram of the fractional difference logistic map. The red dots indicate values of a in the interval $2.7 < a \leq 3.7$, where the trajectory remains at the fixed point (Type-2 values of a) for $N = 15$ and $\mu = 0.8$. Note that the a-axis is shown on the logarithmic scale.

Although it has been reported in the literature that periodic orbits of order higher than period-1 do not exist in fractional difference maps (see Theorem 5 in [39]), it is worthwhile to note that, in the case of finite-precision computations, every non-chaotic trajectory of the fractional difference logistic map will eventually enter a periodic regime. This behaviour is due to a general property of finite-precision implementations [40].

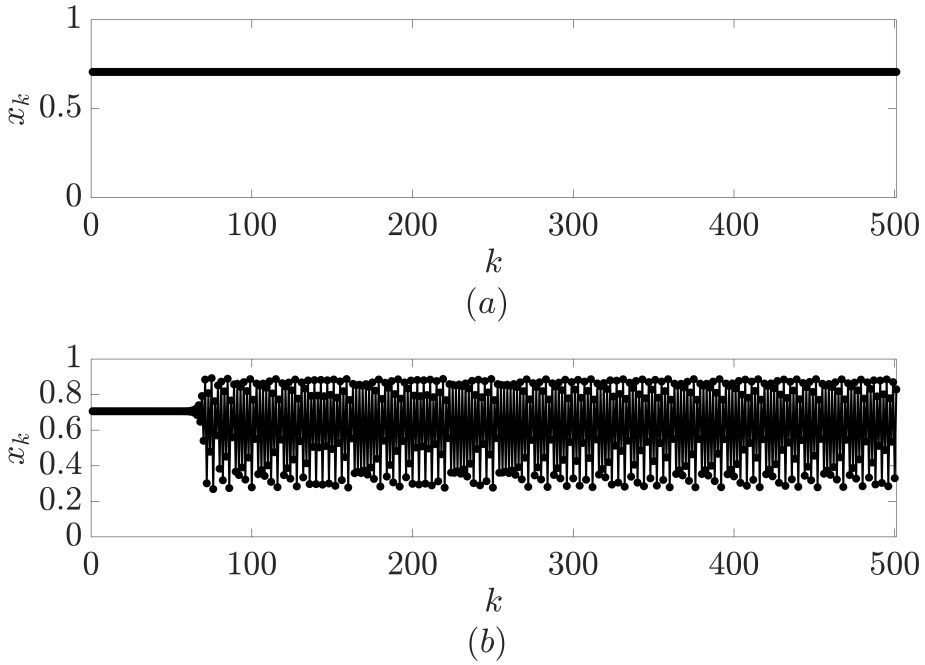

Figure 5. The trajectory starting from $\widetilde{x}_* = 1 - 1/0.340685989097371 \times 10^1$ remains indefinitely at $\widetilde{x}_*$ (panel (**a**)). In contrast, the trajectory starting from $\widetilde{x}_* = 1 - 1/0.340574069915659 \times 10^1$ diverges from $\widetilde{x}_*$ (panel (**b**)). All computations were performed with $N = 15$ and $\mu = 0.8$.

The reported effects induced by finite numerical precision may have significant implications in various applications. A typical example is the stabilization of the unstable fixed point of the nonlinear map presented in [41]. Further investigation into the limitations imposed by numerical precision could provide additional insights into the results presented in [41], particularly if the model would be implemented using experimental electronic circuits.

4. Concluding Remarks

What would happen if the initial condition of the fractional difference logistic map is set exactly to the unstable fixed point (corresponding to the period-1 orbit)? Would the map stay indefinitely at the unstable fixed point, or would it diverge from it?

The answer to this question appears to depend on the accuracy of the floating point arithmetic used in the computational simulation of the investigated fractional difference logistic map.

Insights into the complexity of the issue can be gained by considering the classical logistic map, where the memory horizon is a single backward iteration. It seems that there are three distinct types of parametervalues a which predetermine the behavior of the unstable orbits of the classical logistic map.

The situation is different for the fractional difference logistic map. Firstly, the memory horizon of the fractional difference logistic map reaches the initial condition. Secondly, higher-order orbits do not exist in the fractional difference logistic map. Therefore, the discussion regarding the behavior of the unstable orbits for the fractional difference logistic map is limited only to the fixed point.

It is important to note that we do not make any adjustments to the initial conditions or system parameters. We choose the parameter value that should (theoretically) lead to an unstable orbit and compute the corresponding initial condition (using the available precision). Therefore, we do not make any adjustments, whatever small they could be. All the "adjustments" are automatically and uniquely predetermined by the accuracy of the finite-precision system.

Note that for parameter a values that correspond to a stable period-1 fixed point, the different types of values defined in the paper still exist. While Type-1 and Type-2 values can be observed, Type-3 values act differently: if, for a given a, the analytical value of x_* cannot be represented accurately with a given precision, the system initially diverges away from the approximate value $\widetilde{x}_*$, however, since x_* is stable, the map settles into an orbit that eventually becomes periodic near the fixed point x_*. Due to these effects, the paper mainly considers values of a for which the period-1 fixed point is unstable.

By definition, an unstable fixed point is still an equilibrium. Theoretically, an initial condition that coincides exactly with the unstable fixed point would yield a trajectory that remains at this unstable fixed point forever. One of the major results of this manuscript is that this effect can still hold true in a finite-precision system; however it appears that the underlying reasons for this effect may differ.

This paper provides novel insights into the phenomenon caused by the limitations of finite precision systems. This effect is quantified by introducing three distinct types of initial conditions (it is important to note again that these initial conditions are not artificially perturbed, except for the unavoidable limitations of the finite precision system). The distribution patterns of different types of initial conditions, in relation to the value of the system parameter, are explored. It is demonstrated that such effects can occur well beyond the bifurcation points of the control parameter, which is an interesting result in itself. Moreover, this effect is also quantified with respect to the number of significant digits in the finite-precision system. Finally, these effects are explored for both the classical nonlinear map and its fractional counterpart.

One of the primary advantages of the presented techniques for analyzing precision-related effects in unstable equilibria is a straightforward adaptation for any discrete map using algebraic expressions. In practical problems such as control of fractional discrete maps via temporary stabilization of an unstable orbit [31], knowing whether a given equilibrium is stable or unstable is crucial. Furthermore, if an equilibrium does appear to be unstable, it is important to deduce whether that is due to inherent physical properties of the system or a computational artifact caused to finite precision. However, the techniques also have disadvantages: for example, using the presented techniques for maps featuring transcendental functions (such as the exponential function in the Gauss map [42] for example) would require significant adaptation.

Moreover, it is worth noting that the issue has been considered for different computational precisions (given by the parameter N throughout the paper which denotes decimal significant digits). While such effects have not been explicitly studied in non-decimal computational bases, the principal observations remain the same, though the proportions of Type-1, 2 and 3 points may change.

The behavior of the unstable fixed point of the fractional difference logistic map is similar to that of the unstable fixed point in the classical logistic map (at $N = 15$ and $\mu = 0.8$). If a value of a is randomly chosen from the interval $2.7 < a < 3.7$ (where the fixed point of the fractional difference map is unstable at $\mu = 0.8$), there is approximately a 32% chance that the system will remain at the unstable fixed point indefinitely. Otherwise, the trajectory starting at $\widetilde{x}_*$ will diverge from $\widetilde{x}_*$.

It is worth noting that the divergence from the unstable fixed point of the fractional difference logistic map is a completely computational artifact according to the definition of a fixed point. An ideal computer with $N = \infty$ would always yield trajectories that remain at the fixed point regardless of whether the fixed point is stable or not.

The existence of Type-3 trajectories is predetermined by the finite- precision of the computational framework. A Type-3 trajectory eventually converges to a stable periodic (or chaotic) orbit. It is well known that the convergence to periodic orbits can be either asymptotic or non-asymptotic [43,44]. Therefore, exploring the existence of non-asymptotic convergence to stable orbits directly from unstable fixed points remains a clear objective for future research.

Author Contributions: Conceptualization, M.R., I.T. and T.T.; methodology, I.T. and T.T.; software, E.U. and I.T.; validation, E.U., T.T. and I.T.; formal analysis, M.R.; writing—original draft preparation, E.U., I.T., T.T. and M.R.; writing—review and editing, E.U. and M.R.; visualization, E.U. and I.T.; supervision, M.R. All authors have read and agreed to the published version of the manuscript.

Funding: This research received no external funding.

Data Availability Statement: No new data were created or analyzed in this study. Data sharing is not applicable to this article.

Conflicts of Interest: The authors declare no conflicts of interest.

References

1. Galias, Z. The dangers of rounding errors for simulations and analysis of nonlinear circuits and systems? And how to avoid them. *IEEE Circuits Syst. Mag.* **2013**, *13*, 35–52. [CrossRef]
2. Lozi, R. Can we trust in numerical computations of chaotic solutions of dynamical systems? In *Topology and dynamics of Chaos: In Celebration of Robert Gilmore's 70th Birthday*; World Scientific: Singapore , 2013; pp. 63–98.
3. Klöwer, M.; Coveney, P.V.; Paxton, E.A.; Palmer, T.N. Periodic orbits in chaotic systems simulated at low precision. *Sci. Rep.* **2023**, *13*, 11410. [CrossRef] [PubMed]
4. Hu, T.; Liao, S. On the risks of using double precision in numerical simulations of spatio-temporal chaos. *J. Comput. Phys.* **2020**, *418*, 109629. [CrossRef]
5. Paxton, E.A.; Chantry, M.; Klöwer, M.; Saffin, L.; Palmer, T. Climate modeling in low precision: Effects of both deterministic and stochastic rounding. *J. Clim.* **2022**, *35*, 1215–1229. [CrossRef]
6. Chen, W.; Sun, H.; Li, X. *Fractional Derivative Modeling in Mechanics and Engineering*; Springer: Berlin/Heidelberg, Germany, 2022.
7. Jiang, S.; Zhang, J.; Zhang, Q.; Zhang, Z. Fast evaluation of the Caputo fractional derivative and its applications to fractional diffusion equations. *Commun. Comput. Phys.* **2017**, *21*, 650–678. [CrossRef]
8. Yan, Y.; Sun, Z.Z.; Zhang, J. Fast evaluation of the Caputo fractional derivative and its applications to fractional diffusion equations: A second-order scheme. *Commun. Comput. Phys.* **2017**, *22*, 1028–1048. [CrossRef]
9. May, R.M. Simple mathematical models with very complicated dynamics. *Nature* **1976**, *261*, 459–467. [CrossRef]
10. Ye, G.; Huang, X. An efficient symmetric image encryption algorithm based on an intertwining logistic map. *Neurocomputing* **2017**, *251*, 45–53. [CrossRef]
11. Murillo-Escobar, M.; Cruz-Hernández, C.; Cardoza-Avendaño, L.; Méndez-Ramírez, R. A novel pseudorandom number generator based on pseudorandomly enhanced logistic map. *Nonlinear Dyn.* **2017**, *87*, 407–425. [CrossRef]
12. Groff, J.R. Exploring dynamical systems and chaos using the logistic map model of population change. *Am. J. Phys.* **2013**, *81*, 725–732. [CrossRef]
13. Grassberger, P.; Schreiber, T. Phase transitions in coupled map lattices. *Phys. D Nonlinear Phenom.* **1991**, *50*, 177–188. [CrossRef]
14. Storch, L.S.; Pringle, J.M.; Alexander, K.E.; Jones, D.O. Revisiting the logistic map: A closer look at the dynamics of a classic chaotic population model with ecologically realistic spatial structure and dispersal. *Theor. Popul. Biol.* **2017**, *114*, 10–18. [CrossRef] [PubMed]
15. Ajibade, S.; Chweya, R.; Ogunbolu, M.; Fadipe, S. Utilizing logistic map to enhance the population diversity of PSO. In *Journal of Physics: Conference Series*; IOP Publishing: Bristol, UK, 2022; Volume 2250, p. 012016.
16. Marwan, N.; Wessel, N.; Meyerfeldt, U.; Schirdewan, A.; Kurths, J. Recurrence-plot-based measures of complexity and their application to heart-rate-variability data. *Phys. Rev. E* **2002**, *66*, 026702. [CrossRef] [PubMed]
17. zur Bonsen, A.; Omelchenko, I.; Zakharova, A.; Schöll, E. Chimera states in networks of logistic maps with hierarchical connectivities. *Eur. Phys. J. B* **2018**, *91*, 65. [CrossRef]
18. Abdeljawad, T. On Riemann and Caputo fractional differences. *Comput. Math. Appl.* **2011**, *62*, 1602–1611. [CrossRef]
19. Edelman, M. Caputo standard α-family of maps: Fractional difference vs. fractional. *Chaos Interdiscip. J. Nonlinear Sci.* **2014**, *24*, 023137. [CrossRef]
20. Edelman, M. Fractional maps and fractional attractors. Part II: Fractional difference caputo α-families of maps. *Discontinuity Nonlinearity Complex* **2015**, *4*, 391–402. [CrossRef]
21. He, S.; Zhan, D.; Wang, H.; Sun, K.; Peng, Y. Discrete memristor and discrete memristive systems. *Entropy* **2022**, *24*, 786. [CrossRef]
22. Tarasov, V.E. Discrete map with memory from fractional differential equation of arbitrary positive order. *J. Math. Phys.* **2009**, *50*, 122703. [CrossRef]
23. Danca, M.F. Fractional order logistic map: Numerical approach. *Chaos Solitons Fractals* **2022**, *157*, 111851. [CrossRef]
24. Wang, Y.; Liu, S.; Li, H. On fractional difference logistic maps: Dynamic analysis and synchronous control. *Nonlinear Dyn.* **2020**, *102*, 579–588. [CrossRef]
25. Galias, Z.; Tucker, W. Is the Hénon attractor chaotic? *Chaos Interdiscip. J. Nonlinear Sci.* **2015**, *25*, 033102. [CrossRef] [PubMed]
26. Edelman, M. Evolution of systems with power-law memory: Do we have to die? (Dedicated to the Memory of Valentin Afraimovich). In *Demography of Population Health, Aging and Health Expenditures*; Springer: Cham, Switzerland, 2020; pp. 65–85.

27. Wu, G.C.; Baleanu, D. Discrete fractional logistic map and its chaos. *Nonlinear Dyn.* **2014**, *75*, 283–287. [CrossRef]
28. Munkhammar, J. Chaos in a fractional order logistic map. *Fract. Calc. Appl. Anal.* **2013**, *16*, 511–519. [CrossRef]
29. Peng, Y.; Sun, K.; He, S.; Wang, L. Comments on "Discrete fractional logistic map and its chaos" [Nonlinear Dyn. 75, 283–287 (2014)]. *Nonlinear Dyn.* **2019**, *97*, 897–901. [CrossRef]
30. Edelman, M. Universal fractional map and cascade of bifurcations type attractors. *Chaos Interdiscip. J. Nonlinear Sci.* **2013**, *23*, 033127. [CrossRef]
31. Uzdila, E.; Telksniene, I.; Telksnys, T.; Ragulskis, M. Finite-Time Stabilization of Unstable Orbits in the Fractional Difference Logistic Map. *Fractal Fract.* **2023**, *7*, 570. [CrossRef]
32. Danca, M.F.; Fečkan, M.; Kuznetsov, N. Chaos control in the fractional order logistic map via impulses. *Nonlinear Dyn.* **2019**, *98*, 1219–1230. [CrossRef]
33. Yabuki, M.; Tsuchiya, T. Double precision computation of the logistic map depends on computational modes of the floating-point processing unit. *arXiv* **2013**, arXiv:1305.3128.
34. Galias, Z. Periodic orbits of the logistic map in single and double precision implementations. *IEEE Trans. Circuits Syst. II Express Briefs* **2021**, *68*, 3471–3475. [CrossRef]
35. Shonkwiler, R.W.; Mendivil, F. *Explorations in Monte Carlo Methods*; Springer: Berlin/Heidelberg, Germany, 2009.
36. Tsuchiya, T.; Yamagishi, D. The complete bifurcation diagram for the logistic map. *Z. Naturforschung A* **1997**, *52*, 513–516. [CrossRef]
37. Diblík, J.; Fečkan, M.; Pospíšil, M. Nonexistence of periodic solutions and S-asymptotically periodic solutions in fractional difference equations. *Appl. Math. Comput.* **2015**, *257*, 230–240. [CrossRef]
38. Edelman, M. Stability of fixed points in generalized fractional maps of the orders $0< \alpha< 1$. *Nonlinear Dyn.* **2023**, *111*, 10247–10254.
39. Bhalekar, S.; Gade, P.M. Fractional-order periodic maps: Stability analysis and application to the periodic-2 limit cycles in the nonlinear systems. *J. Nonlinear Sci.* **2023**, *33*, 119. [CrossRef]
40. Li, C.; Feng, B.; Li, S.; Kurths, J.; Chen, G. Dynamic analysis of digital chaotic maps via state-mapping networks. *IEEE Trans. Circuits Syst. Regul. Pap.* **2019**, *66*, 2322–2335. [CrossRef]
41. Sadeghian, H.; Merat, K.; Salarieh, H.; Alasty, A. On the fuzzy minimum entropy control to stabilize the unstable fixed points of chaotic maps. *Appl. Math. Model.* **2011**, *35*, 1016–1023. [CrossRef]
42. Hilborn, R.C. *Chaos and Nonlinear Dynamics: An Introduction for Scientists and Engineers*; Oxford University Press: Oxford, UK, 2000.
43. Petkevičiūtė-Gerlach, D.; Timofejeva, I.; Ragulskis, M. Clocking convergence of the fractional difference logistic map. *Nonlinear Dyn.* **2020**, *100*, 3925–3935. [CrossRef]
44. Timofejeva, I.; Laukaitis, G.; Rinkevicius, Z.; Ragulskis, M. Finite-time stabilization of the fractional model of the driven dissipative nonlinear pendulum. *Int. J. Bifurc. Chaos* **2022**, *32*, 2250056. [CrossRef]